LETTERS

Visualizing spatially correlated dynamics that directs RNA conformational transitions

Qi Zhang[1], Andrew C. Stelzer[1], Charles K. Fisher[1] & Hashim M. Al-Hashimi[1]

RNAs fold into three-dimensional (3D) structures that subsequently undergo large, functionally important, conformational transitions in response to a variety of cellular signals[1–3]. RNA structures are believed to encode spatially tuned flexibility that can direct transitions along specific conformational pathways[4,5]. However, this hypothesis has proved difficult to examine directly because atomic movements in complex biomolecules cannot be visualized in 3D by using current experimental methods. Here we report the successful implementation of a strategy using NMR that has allowed us to visualize, with complete 3D rotational sensitivity, the dynamics between two RNA helices that are linked by a functionally important trinucleotide bulge over timescales extending up to milliseconds. The key to our approach is to anchor NMR frames of reference onto each helix and thereby directly measure their dynamics, one relative to the other, using 'relativistic' sets of residual dipolar couplings (RDCs)[6,7]. Using this approach, we uncovered super-large amplitude helix motions that trace out a surprisingly structured and spatially correlated 3D dynamic trajectory. The two helices twist around their individual axes by approximately 53° and 110° in a highly correlated manner ($R = 0.97$) while simultaneously ($R = 0.81$–0.92) bending by about 94°. Remarkably, the 3D dynamic trajectory is dotted at various positions by seven distinct ligand-bound conformations of the RNA. Thus even partly unstructured RNAs can undergo structured dynamics that directs ligand-induced transitions along specific predefined conformational pathways.

Although advances in solution NMR methods are providing rare insights into the atomic details of internal motions in biomolecules[8–11], the 3D visualization of atomic movements remains hampered by the fact that common NMR measurements do not probe the dynamics of bond vectors relative to one another, but rather, relative to the external magnetic field. Reliance on a single external frame of reference reduces the possibilities for overcoming fundamental spatial sensitivity limitations associated with axially symmetric interactions, makes it impossible to establish spatial correlations between motions occurring at different sites, and renders characterization of internal motions only possible if their spectroscopic contributions can be disentangled from those due to the much larger overall brownian motions[12]. The last proves intractable when domains in multi-domain systems move collectively and lead to correlated changes in the overall motions, as is generally encountered when A-form helices move in RNA[13].

We transformed the basic NMR experiment by anchoring frames of reference onto individual RNA helices and thereby measuring their dynamics directly as motions of one helix relative to the other by using multiple sets of RDCs. The frames were anchored using a generally applicable method which involves elongating helices[13] so that they dominate overall alignment of the elongated RNA in ordering media, with the elongated axis being on average oriented parallel to the magnetic field (Fig. 1a). This effectively disentangles helix motions from overall alignment and renders RDCs dependent on the angle (Ω) between bond vectors and the internal elongated axis, and not a detached external magnetic field. By anchoring the frame of reference onto different helices, the same helix motions can be measured from different helix-centred perspectives, opening a new avenue for extending the achievable spatial sensitivity with which motions can be characterized. For example, although RDCs probe inter-helical bending (β) and twisting (α) motions of the short helix, they are insensitive to twisting motions (γ) around the axially

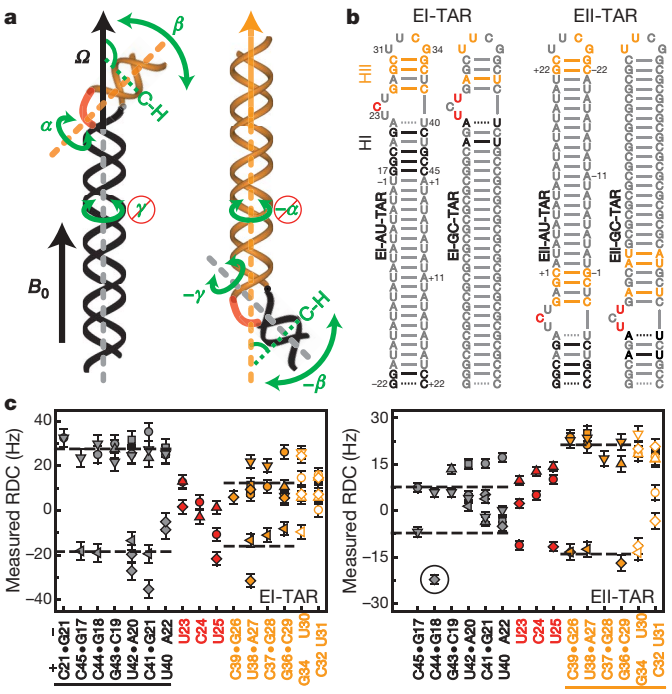

Figure 1 | Measurement of RNA helix motions in 3D using helix-anchored frames and RDCs. a, NMR reference frames are anchored by elongating helices so that the RNA aligns with the elongated axis, being on average oriented parallel to the magnetic field (B_0). **b**, Independent elongation of HI and HII in TAR using a strategy that renders elongation residues NMR invisible[13]. $^{13}C/^{15}N$ labelled and unlabelled nucleotides are shown in colour and grey, respectively. **c**, The C1′H1′ (diamond), C2H2 (square), C5H5 (circle), C6H6 (triangle up), C8H8 (triangle down) and N1/3H1/3 (triangle left) RDCs as a function of the TAR secondary structure. Elongated helices are underlined. The horizontal dashed lines correspond to the average positive or negative RDC value in each helix. Error bars represent experimental uncertainty (one s.d.) estimated from duplicate measurements and analysis of signal-to-noise and line widths.

[1]Department of Chemistry and Biophysics, University of Michigan, 930 North University Avenue, Ann Arbor, Michigan 48109-1055, USA.

symmetric elongated helix (Fig. 1a). This vanishing sensitivity can be resurrected, and helix motions thereby measured with complete 3D rotational sensitivity, by inverting which helix is elongated and measuring RDCs that probe the angles β and γ but not α (Fig. 1a). By measuring motions in this relativistic manner, the helix-anchored frames also allow spatial correlations between motions of two or more helices to be directly established. A similar strategy can be implemented without the need for helix elongation through analytical treatment of couplings between helix motions and overall magnetic alignment of the non-elongated RNA[14].

The transactivation response element (TAR) RNA (Fig. 1b) from the human immunodeficiency virus type-1 (HIV-1) is a major drug target and a paradigm for understanding ligand-induced RNA conformational transitions. Numerous studies have shown that HIV-1 TAR undergoes dramatic conformational rearrangements involving large rigid-body movements of its two helical domains (averaging 42° and as large as 71°) that allow it to bind diverse targets in and around the bulge, including peptide derivatives of its cognate protein Tat[15–17], divalent ions[18] and five, different, small molecules that inhibit the TAR–Tat interaction[19–22]. We recently reported evidence based on elongation of helix I and NMR spin relaxation measurements[13] for diffusion-limited collective helix motions in TAR occurring at timescales of less than 19 ns. Here, we apply our double-elongation RDC approach to visualize the TAR helix motions in 3D over timescales extending up to milliseconds.

Each of the two helices in TAR was independently elongated (EI-TAR and EII-TAR) by using a generally applicable 'NMR invisible' strategy[13] which entailed preparation of four E-TAR constructs (Fig. 1b). RDCs were measured by using Pf1 phage (approximately 6–8 mg ml^{-1}) as an ordering medium[23]. Comparison of NMR chemical shifts indicated that domain elongation and the introduction of Pf1 phage do not significantly perturb the inter-helical conformational dynamics and functional properties of TAR (Supplementary Fig. 1). Inspection of the raw RDCs measured in E-TAR immediately revealed evidence for collective helix motions (Fig. 1c). In both EI-TAR and EII-TAR, the RDCs measured for differently oriented bond vectors in the short helices were significantly smaller (on average by about 55% and about 40%, respectively) than corresponding values measured in the elongated helices (the circled RDC in EII-TAR is consistent with this trend; the large value arises because the bond vector is oriented uniquely parallel to long axis of helix II (HII)) (Fig. 1c). This indicated that the short helices align to a lesser extent than their elongated counterparts because they undergo collective helix motions at sub-millisecond timescales. The small RDCs observed at the bulge are also consistent with previous findings showing that the inter-helical linker is highly flexible[13]. As expected, the collective helix motional amplitudes and thus the observed gap in helix RDCs were significantly diminished after complexation with the ligand argininamide (ARG), which has previously been shown to stabilize the relative alignment of the two TAR helices[13] and upon shortening the bulge linker through deletion of residue C24 (Supplementary Fig. 2).

Domain-elongation allowed us to analyse the RDCs by using a model-free order-tensor analysis (Supplementary Information)[24,25] from which we obtained geometrical information about the inter-helical motional trajectory. The RDCs and previously validated idealized A-form helix geometry[26] were used to determine five order-tensor elements[27] describing ordering of each helix relative to the external magnetic field, or in the case of elongated RNA, relative to the internal elongated helix axis. An excellent RDC fit was obtained in each case, confirming that the helices also adopt the idealized A-form geometry in the elongated TAR context (Fig. 2a). The order tensors obtained for the elongated helices show that they align in the expected axially symmetric manner ($\eta \approx 0$, ranges between 0 and 1 for minimum and maximum motional asymmetry), with their elongated axis (z direction) oriented on average nearly parallel to the magnetic field (S_{zz}, deviations fewer than six degrees) (Fig. 2b).

The order tensors obtained for the short helices, on the other hand, provided insights into their orientational dynamics relative to the elongated helices (Fig. 2c). According to the short HII order tensor, the long axis (S_{zz}) of HI is on average inclined at an inter-helical bend angle of approximately 25° (Fig. 2c). In contrast, the same bend angle is approximately 54° according to the short HI order tensor (Fig. 2c). These contrasting views of the same inter-helical angle suggest the presence of twisting motions that alter how each helix views the other's average orientation. The very high degree of attenuation in the level of order (ϑ)[25] observed for the two short helices compared with their elongated counterparts ($\vartheta_{int} = \vartheta_{short}/\vartheta_{elongated} \approx 0.45 \pm 0.05$ and 0.47 ± 0.02 for EI-TAR and EII-TAR, respectively, and ranges between 0 and 1 for maximum and minimum motions) confirmed the presence of super-large amplitude helix motions that significantly exceed the amplitudes observed previously by spin relaxation ($\sqrt{S_s^2} = \vartheta_{int} \approx 0.86 \pm 0.02$)[13]. Similar motional amplitudes were observed when anchoring the frames of reference in non-elongated TAR by using motional couplings[14].

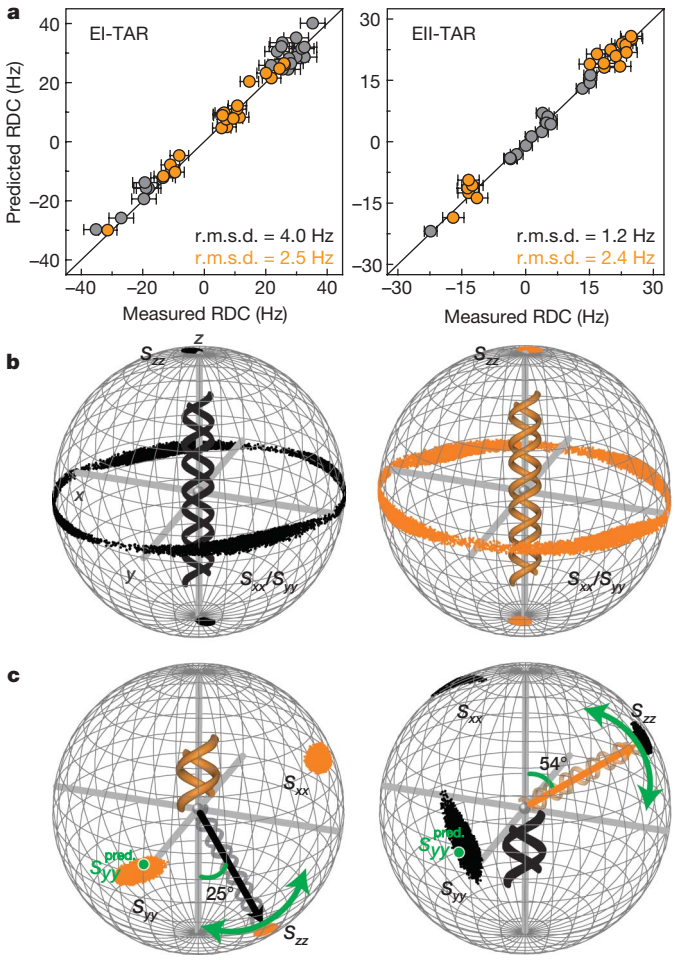

Figure 2 | Helix motions from model-free order-tensor analysis of RDCs. **a**, Comparison of RDCs measured in HI (black) and HII (orange) in EI-TAR and EII-TAR with values back-predicted by using the best-fit order tensor and an idealized A-form helix geometry[26]. Shown are the root mean squared deviations (r.m.s.d.) between measured and predicted RDCs. Error bars indicate the s.d. **b, c**, Globes showing the orientation of the order-tensor frames determined for the (**b**) elongated and (**c**) short helices in EI-TAR and EII-TAR. Solutions are depicted relative to a molecular frame in which HI and HII are coaxial with the helix axis oriented along the z direction. Green circles are the S_{yy} direction predicted for an inter-helix motional model involving inter-conversion among seven equally populated ligand-bound TAR conformations.

Given the broader timescale sensitivity of RDCs (less than 0.1 ms) compared with spin relaxation (less than 19 ns) and that qualitative analysis of the TAR resonance intensities provides no evidence for significant exchange broadening in and around the bulge[13], the motions likely represent large-scale diffusive dynamics occurring at the nanosecond to microsecond timescale and not microsecond to millisecond transitions between discrete sub-states. As expected, considerably smaller inter-helix motional amplitudes were observed in the EI-TAR+ARG complex ($\vartheta_{int} = 1.09 \pm 0.08$ and $S_s = 1$) or after deletion of bulge residue C24 ($\vartheta_{int} = 0.77 \pm 0.04$ and $S_s = 0.94 \pm 0.02$). Surprisingly, these very large amplitude helix motions observed in E-TAR are not spatially random as both short helices report a high degree of motional asymmetry ($\eta \approx 0.44$, Supplementary Table 2) and a preference for inter-helical bending through rotations around a principal direction (S_{yy}) that is nearly orthogonal to both helical axes (Fig. 2c). Remarkably, a virtually identical axis of motional asymmetry (Fig. 2c, in green circles) relates the orientation of TAR helices in seven distinct ligand-bound conformations[16–22], suggesting fundamental spatial similarities between how the helices move in free TAR and how they move when adapting to bind different targets. In contrast, the motions observed following deletion of bulge residue C24 in EI-TAR appear to be more spatially isotropic ($\eta \approx 0.07$) suggesting that the length of the bulge codes for both the amplitude and directionality of the helix motions.

To visualize the spatially non-random inter-helical motions, we performed a search over ensembles[28] with up to three ($N = 3$) equally populated inter-helical conformers that can reproduce the nine independent parameters afforded by the RDCs (Supplementary Information). The conformers within an ensemble define key loci along the trajectory that serve to capture its essential 3D spatial features even if the trajectory was to involve many more conformations. Loose steric constraints were also implemented in the conformational search (Supplementary Information). In the case of TAR, both the $N = 1$ and $N = 2$ searches yielded a very poor RDC fit, confirming the existence of an inter-helix motional trajectory that is more complex than a simple two-state jump. In contrast, a very good fit was obtained for $N = 3$, with insignificant improvements obtained with $N = 4$ (Fig. 3a).

Cluster analysis of the $N = 3$ ensemble solutions revealed two RDC-degenerate solutions (A and B) that differ primarily in whether helices in the three conformers twist in a clockwise (A) or anticlockwise (B) manner (Fig. 3b). A remarkable feature common to both solutions is that the three conformers fall nearly along a straight line in the 3D inter-helix Euler space defining twisting around each helix (α and $-\gamma$) and inter-helical bending (β) (Fig. 3b). This 3D linear trajectory cannot be traced out by a 'single axis rotation', explaining why a two-state jump does not yield an acceptable RDC fit. It suggests that the two helices twist and bend in a highly correlated manner. Although we cannot exclude the possibility that ensembles A and B co-exist with equal populations as this yields an equally good E-TAR RDC fit, cross-validation against an independent set of phage-induced RDCs measured in non-elongated TAR[29] strongly argues in favour of ensemble A over ensemble B or combination of A and B (Supplementary Information). The A ensemble, which also yields good agreement with magnetic-field-induced RDCs measured in non-elongated TAR[14], gives rise to a motional trajectory in which HI and HII twist by approximately 53° and approximately 110°, respectively, in a highly synchronized manner ($R = 0.97$) while simultaneously ($R = 0.81$–0.92) bending by about 94° (Fig. 3c, Supplementary Movie 1).

Visualization of the TAR inter-helical trajectory allowed us to examine directly its potential role in directing ligand-induced structural transitions. Specifically, it allowed us to test directly the possibility that ligands bind to existing TAR conformations by 'tertiary capture'[4,5]. Remarkably, we find that the seven bound TAR conformations fall along various positions of the A dynamical trajectory (Fig. 4a). The bound conformers also trace out a similar linear trajectory in the 3D inter-helix Euler space ($R = 0.70$–0.82), confirming that correlated dynamics is an intrinsic property of the TAR structure (Fig. 4a). The TAR dynamical envelope encapsulates nearly all of the ligand-bound conformations (Fig. 4b, Supplementary Movie 2), indicating that ligands can induce the TAR structural transitions by capturing existing conformers along various positions of the free RNA dynamical trajectory. Thus a highly flexible RNA can be spatially tuned to undergo structured motions that direct functional transitions along specific pathways. The presented NMR strategy provides a general approach to characterize collective movements of helices and other locally well defined RNA sub-fragments across a variety of functionally important junctions with 3D spatial resolution.

METHODS SUMMARY

E-TAR samples (approximately 0.6–1.0 mM) were prepared by *in vitro* transcription as described previously[13]. All experiments were conducted in NMR buffer (15 mM sodium phosphate, 25 mM sodium chloride, 0.1 mM EDTA,

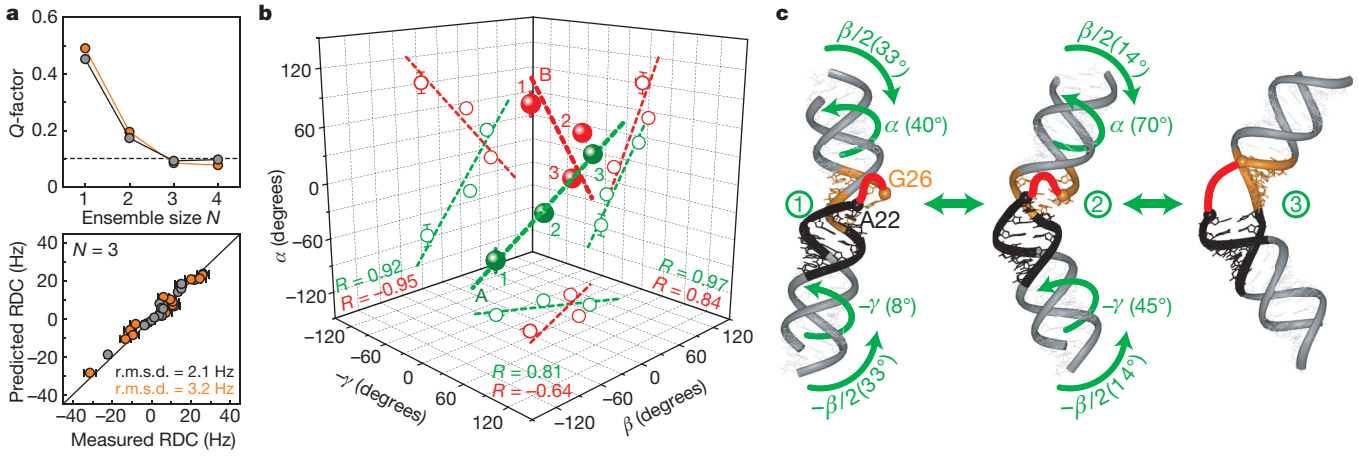

Figure 3 | Visualizing TAR inter-helical motions in 3D. a, Quality factor (Q)[31] for HI (black) and HII (orange) as a function of the inter-helical ensemble size N (top panel). The horizontal dashed line corresponds to the expected value of Q given experimental uncertainty. Comparison of the RDCs measured in short HI (black) and HII (orange), and values back-predicted by using the best-fit ($N = 3$) dynamical ensemble A (bottom panel). **b**, The best-fit TAR ensembles A (green) and B (red) in which each conformer (1, 2 and 3) is specified by three Euler angles defining twisting around HI ($-\gamma$), HII (α) and inter-helical bending (β). The 3D best-fit line is shown with its 2D projections along each plane and the associated correlation coefficient (R). **c**, The three TAR conformers in ensemble A. Helices are elongated for clarity. Error bars indicate the s.d.

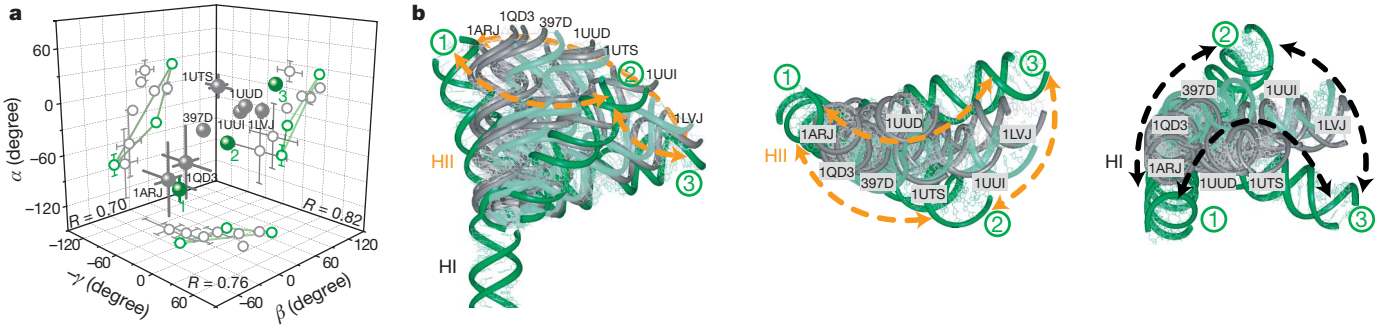

Figure 4 | Correlated TAR dynamics steer ligand-induced transitions. **a**, The three TAR dynamical conformers (green) and the TAR conformation (grey) bound to peptide derivatives of Tat (1ARJ)[16,17], divalent ions (397D)[18] and five different small molecules (1QD3, 1LVJ, 1UUD, 1UUI, 1UTS)[19–22]. Shown on each 2D plane is the correlation coefficient (R) between angles for the ligand-bound conformations. For bound structures, the s.d. is over the family of reported NMR models. Only one model was reported in structures 397D, 1UUI and 1UUD; thus no s.d. is reported. **b**, Comparison of the three TAR dynamical conformers (green) and ligand-bound TAR conformations (grey). Sub-conformers along the linear pathway linking conformers 1→2, 2→3 and 3→1 are shown in light green, and the direction of the trajectory is shown with arrows. Horizontal view following superposition of HI (left panel), vertical view down and up the helix axis of HI (middle panel) and HII (right panel) following superposition of HI and HII, respectively.

and pH approximately 6.4) at 298 K on an Avance Bruker 600 MHz NMR spectrometer equipped with a triple-resonance 5 mm cryogenic probe, and for the EI-TAR+ARG complex on a Varian Inova 800 MHz NMR spectrometer equipped with a 5 mm triple-resonance probe. The base ^{1}H–^{13}C splittings were measured from the difference between the upfield and downfield components of the ^{1}H–^{13}C doublet along the ^{1}H dimension using the narrow transverse relaxation-optimized spectroscopy (TROSY) component in the ^{13}C dimension as implemented in 2D ^{1}H–^{13}C S^{3}CT-heteronuclear single-quantum correlation (HSQC) experiments[30]. The ^{1}H–^{15}N splittings were measured in duplicate by using standard HSQC experiments without decoupling in the indirect or direct dimension. RDCs measured in E-AU-TAR and E-GC-TAR were normalized as detailed in Methods to take into account small differences in the degree of alignment arising from use of a slightly different Pf1 phage concentration[23]. The normalized RDCs were combined in the order-tensor analysis. Errors in the helix order tensors due to RDC uncertainty and A-form 'structural noise' were computed using the program AFORM-RDC[26]. Idealized A-form helices were constructed by using Insight II (Molecular Simulations, Inc.), noting that the propeller twist angles had to be corrected from +15° to the standard A-form value of −15° (ref. 26). The ensemble search was performed by using software written in-house as detailed in Methods. The Euler angles (α, β, γ) used in this work follow the γ-convention and transform the HII frame from an alignment that is perfectly coaxial with HI, with the helix axis oriented along the molecular z direction to the final orientation in the conformer. Positive angles correspond to anti-clockwise rotations, and positive α and γ angles correspond to under- and over-twisting of HII and HI, respectively.

Full Methods and any associated references are available in the online version of the paper at www.nature.com/nature.

Received 19 July; accepted 18 October 2007.

1. Micura, R. & Hobartner, C. On secondary structure rearrangements and equilibria of small RNAs. *ChemBioChem* **4**, 984–990 (2003).
2. Schroeder, R., Barta, A. & Semrad, K. Strategies for RNA folding and assembly. *Nature Rev. Mol. Cell Biol.* **5**, 908–919 (2004).
3. Schwalbe, H. *et al.* Structures of RNA switches: insight into molecular recognition and tertiary structure. *Angew. Chem. Int. Edn Engl.* **46**, 1212–1219 (2007).
4. Leulliot, N. & Varani, G. Current topics in RNA-protein recognition: control of specificity and biological function through induced fit and conformational capture. *Biochemistry* **40**, 7947–7956 (2001).
5. Al-Hashimi, H. M. Dynamics-based amplification of RNA function and its characterization by using NMR spectroscopy. *ChemBioChem* **6**, 1506–1519 (2005).
6. Tjandra, N. & Bax, A. Direct measurement of distances and angles in biomolecules by NMR in a dilute liquid crystalline medium. *Science* **278**, 1111–1114 (1997).
7. Tolman, J. R., Flanagan, J. M., Kennedy, M. A. & Prestegard, J. H. NMR evidence for slow collective motions in cyanometmyoglobin. *Nature Struct. Biol.* **4**, 292–297 (1997).
8. Furtig, B. *et al.* Time-resolved NMR studies of RNA folding. *Biopolymers* **86**, 360–383 (2007).
9. Blackledge, M. Recent progress in the study of biomolecular structure and dynamics in solution from residual dipolar couplings. *Prog. Nucl. Magn. Reson. Spectrosc.* **46**, 23–61 (2005).
10. Mittermaier, A. & Kay, L. E. New tools provide new insights in NMR studies of protein dynamics. *Science* **312**, 224–228 (2006).
11. Palmer, A. G. III & Massi, F. Characterization of the dynamics of biomacromolecules using rotating-frame spin relaxation NMR spectroscopy. *Chem. Rev.* **106**, 1700–1719 (2006).
12. Bruschweiler, R. New approaches to the dynamic interpretation and prediction of NMR relaxation data from proteins. *Curr. Opin. Struct. Biol.* **13**, 175–183 (2003).
13. Zhang, Q., Sun, X., Watt, E. D. & Al-Hashimi, H. M. Resolving the motional modes that code for RNA adaptation. *Science* **311**, 653–656 (2006).
14. Zhang, Q. & Al-Hashimi, H. M. Extending the NMR spatial resolution limit by motional couplings. *Nature Methods* (submitted).
15. Aboul-ela, F., Karn, J. & Varani, G. Structure of HIV-1 TAR RNA in the absence of ligands reveals a novel conformation of the trinucleotide bulge. *Nucleic Acids Res.* **24**, 3974–3981 (1996).
16. Puglisi, J. D. *et al.* Conformation of the TAR RNA-arginine complex by NMR spectroscopy. *Science* **257**, 76–80 (1992).
17. Aboul-ela, F., Karn, J. & Varani, G. The structure of the human-immunodeficiency-virus type-1 Tar RNA reveals principles of RNA recognition by Tat protein. *J. Mol. Biol.* **253**, 313–332 (1995).
18. Ippolito, J. A. & Steitz, T. A. A 1.3-angstrom resolution crystal structure of the HIV-1 trans- activation response region RNA stem reveals a metal ion-dependent bulge conformation. *Proc. Natl Acad. Sci. USA* **95**, 9819–9824 (1998).
19. Faber, C., Sticht, H., Schweimer, K. & Rosch, P. Structural rearrangements of HIV-1 Tat-responsive RNA upon binding of neomycin B. *J. Biol. Chem.* **275**, 20660–20666 (2000).
20. Du, Z., Lind, K. E. & James, T. L. Structure of TAR RNA complexed with a Tat–TAR interaction nanomolar inhibitor that was identified by computational screening. *Chem. Biol.* **9**, 707–712 (2002).
21. Davis, B. *et al.* Rational design of inhibitors of HIV-1 TAR RNA through the stabilisation of electrostatic 'hot spots'. *J. Mol. Biol.* **336**, 343–356 (2004).
22. Murchie, A. I. *et al.* Structure-based drug design targeting an inactive RNA conformation: exploiting the flexibility of HIV-1 TAR RNA. *J. Mol. Biol.* **336**, 625–638 (2004).
23. Hansen, M. R., Mueller, L. & Pardi, A. Tunable alignment of macromolecules by filamentous phage yields dipolar coupling interactions. *Nature Struct. Biol.* **5**, 1065–1074 (1998).
24. Meiler, J. *et al.* Model-free approach to the dynamic interpretation of residual dipolar couplings in globular proteins. *J. Am. Chem. Soc.* **123**, 6098–6107 (2001).
25. Tolman, J. R., Al-Hashimi, H. M., Kay, L. E. & Prestegard, J. H. Structural and dynamic analysis of residual dipolar coupling data for proteins. *J. Am. Chem. Soc.* **123**, 1416–1424 (2001).
26. Musselman, C. *et al.* Impact of static and dynamic A-form heterogeneity on the determination of RNA global structural dynamics using NMR residual dipolar couplings. *J. Biomol. NMR* **36**, 235–249 (2006).
27. Saupe, A. Recent results in the field of liquid crystals. *Angew. Chem. Int. Edn Engl.* **7**, 97–112 (1968).
28. Clore, G. M. & Schwieters, C. D. Amplitudes of protein backbone dynamics and correlated motions in a small alpha/beta protein: correspondence of dipolar coupling and heteronuclear relaxation measurements. *Biochemistry* **43**, 10678–10691 (2004).
29. Al-Hashimi, H. M. *et al.* Concerted motions in HIV-1 TAR RNA may allow access to bound state conformations: RNA dynamics from NMR residual dipolar couplings. *J. Mol. Biol.* **315**, 95–102 (2002).

30. Meissner, A. & Sorensen, O. W. The role of coherence transfer efficiency in design of TROSY- type multidimensional NMR experiments. *J. Magn. Reson.* **139,** 439–442 (1999).
31. Cornilescu, G., Marquardt, J. L., Ottiger, M. & Bax, A. Validation of protein structure from anisotropic carbonyl chemical shifts in a dilute liquid crystalline phase. *J. Am. Chem. Soc.* **120,** 6836–6837 (1998).

Supplementary Information is linked to the online version of the paper at www.nature.com/nature.

Acknowledgements We thank A. Kurochkin for NMR expertise. We acknowledge the Michigan Economic Development Cooperation and the Michigan Technology Tri-Corridor for the support of the purchase of a 600 MHz spectrometer, and the W. F. Keck Foundation, National Science Foundation (NSF) and National Institutes of Health (NIH) for funds for the purchase of an 800 MHz spectrometer. Supported by an NIH and NSF grant.

Author Contributions H.M.A. conceived the technique, Q.Z. and H.M.A. analysed the data and wrote the paper. Q.Z., C.K.F. and H.M.A. analysed the HIV-2 TAR data. Q.Z., A.C.S. and C.K.F. prepared the samples and performed the NMR experiments.

Author Information Supplementary Movies are hosted at the publicly accessible Database of Macromolecular Movements (http://www.molmovdb.org/). Reprints and permissions information is available at www.nature.com/reprints. Correspondence and requests for materials should be addressed to H.M.A. (hashimi@umich.edu).

METHODS

Normalization of RDCs. The RDCs (Supplementary Table 1) were measured independently for HIV-1 EI-AU-TAR, EI-GC-TAR, HIV-2 EI-AU-TAR and EI-GC-TAR by using approximately 8 mg ml^{-1} Pf1 phage and for HIV-1 EII-AU-TAR, EII-GC-TAR, EI-AU-TAR+ARG and EI-GC-TAR+ARG using approximately 6 mg ml^{-1} Pf1 phage ordering medium[23]. The E-AU-TAR and E-GC-TAR RDCs were normalized before combination in the order-tensor analysis by repeatedly fitting the RDCs to each helix after uniform scaling of the E-GC-TAR RDCs by a normalization factor L. For EI-TAR, EII-TAR, EI-TAR+ARG and HIV-2 EI-TAR, the two helices yielded a similar best-fit L value of 0.84 (0.82 for HI and 0.85 for HII), 0.97 (0.97 for both HI and HII), 0.75 (0.71 for HI and 0.79 for HII) and 1.01 (1.01 for both HI and HII), respectively. Insignificant variations were observed in the order-tensor analysis and the ensemble search when varying L by ± 0.05.

Computing inter-helix Euler angles. Euler angles for the bound TAR structures (Fig. 4a) were computed as follows. Idealized A-form helices were constructed by using Insight II (Molecular Simulations, Inc.) (propeller twist angles had to be corrected from $+15^\circ$ to -15°) and superimposed onto the two helices of the bound TAR structures (PDB ID 1ARJ, 397D, 1LVJ, 1QD3, 1UUD, 1UUI and 1UTS), excluding terminal residues 17 and 45 when superimposing helices to HI. The inter-helix Euler angles (α, β, γ) were then computed by using EulerRNA[32] and a molecular frame in which the HI helix was oriented along the z direction with the 5′ and 3′ ends along the negative and positive z direction, respectively.

Computing axis of asymmetry for ligand-bound conformations. The S_{yy} principal direction (Fig. 2c) was computed as follows. Idealized A-form helices were superimposed onto the helices of the bound TAR structures as described above. Synthetic RDCs were computed for each helix by using the experimental order tensor determined for the elongated helices (Supplementary Table 2). The synthetic short helix RDCs were then averaged over the seven bound structures assuming equal populations and used to determine order tensors for each helix by using the same procedure used to determine the experimental order tensors shown in Fig. 2c.

Ensemble search. The ensemble search was performed by using in-house software. Trial inter-helical orientations defined by the inter-helix Euler angles α, β, γ were generated, and RDCs computed for each of the two short helices using the order tensors determined for their corresponding elongated helices (Supplementary Table 2). The predicted RDCs were then compared with measured counterparts, either directly ($N = 1$) or after 'dynamical' averaging over two ($N = 2$) or more ($N \geq 3$) trial conformations. Specifically, Q factors[31] were computed for each helix (Q_{HI} and Q_{HII}) and for the helices combined $Q^{\mathrm{tot}} = ((Q^2_{\mathrm{HI}} + Q^2_{\mathrm{HII}})/2)^{1/2}$ using the degree of order for elongated helices in the normalization: $Q_{\mathrm{HI(HII)}} = \left(\sum_i \left(\mathrm{RDC}_i^{\mathrm{meas}} - \mathrm{RDC}_i^{\mathrm{pred}} \right)^2 / \sum_i \left(D^2_{\mathrm{max},i} S^2_{\mathrm{zzEII(EI)}} (3 + \eta^2_{\mathrm{EII(EI)}})/15 \right) \right)^{1/2}$, $D_{\mathrm{max}} = -\frac{\mu_0 \gamma_m \gamma_n h}{8\pi^3 r^3_{m,n}}$ and $\eta = \frac{S_{xx} - S_{yy}}{S_{zz}}$.

The distance between C39 O3′ and U40 P was maintained at 1.60 Å. Loose steric constraints were imposed by excluding conformations that lead to: (i) van der Waals collisions between the two A-form helices, using uniform and conservative van der Waals radii of 2.5 Å excluding protons as well as all the terminal A22-U40 base pair (the latter was used to allow deformations in this more flexible region of the A-form structure to take place); and (ii) a distance between A22 O3′ and G26 P that is greater than the theoretically allowed length of the trinucleotide bulge (21 Å)[33]. The ensemble search was conducted in two stages. In the first stage, an exhaustive grid search over the 3- ($N = 1$), 6- ($N = 2$) or 9- ($N = 3$) dimensional α, β, γ parameter space was performed using step-size angles of $\alpha = 20^\circ$, $\beta = 10^\circ$ and $\gamma = 20^\circ$. Solutions with $Q_{\mathrm{HI}} \leq Q^{\mathrm{I}}$ and $Q_{\mathrm{HII}} \leq Q^{\mathrm{II}}$ were subjected to a second round of refinement. Q^{I} and Q^{II} were determined by Monte-Carlo-type simulations. Briefly, the average Q value was computed after the imposition of (i) inter-helix 'structural noise' in each conformer consisting of rotations with step-size angles $\alpha = 20^\circ$, $\beta = 10^\circ$, $\gamma = 20^\circ$, and (ii) RDC uncertainty (about 3.4 Hz and about 1.9 Hz for EI-TAR and EII-TAR, respectively; note the smaller RDC error in EII-TAR is attributed to its approximate 41% smaller degree of alignment compared with EI-TAR (Supplementary Table 2)). For $N = 1$, all solutions were subjected to a second round of refinement. For $N > 1$, 10% of the accepted ensembles yielding the lowest Q^{tot} values and another randomly chosen 10% were subjected to further rounds of refinement. In the second stage, each ensemble was further refined by performing a narrower search over its three conformers. This was accomplished by perturbing the original inter-helix Euler α, β, γ angles defining each conformer by $\alpha = \pm 20^\circ$, $\beta = \pm 10^\circ$, $\gamma = \pm 20^\circ$ in increments of 10°, 5° and 10°, respectively. The best-fit solution yielding the lowest Q^{tot} value was then subjected to two additional rounds of refinement involving increasingly smaller perturbations: $\alpha = \pm 10^\circ$, $\beta = \pm 5^\circ$, $\gamma = \pm 10^\circ$, in increments of 5°, 2.5° and 5°, respectively; and finally $\alpha = \pm 5^\circ$, $\beta = \pm 2.5^\circ$, $\gamma = \pm 5^\circ$, in increments of 2.5°, 1.25° and 2.5°, respectively. Final ensemble solutions were accepted if both Q_{HI} and $Q_{\mathrm{HII}} \leq Q^{\mathrm{final}}$, where Q^{final} takes into account A-form structural noise and RDC uncertainty ($Q = 7.5\%$), uncertainty in the order tensors determined for the elongated helices ($Q = 6.2\%$) and finite step size in the final round of refinement ($Q = 2.9\%$). For $N = 3$, the value of Q^{final} was 10.2%. The performance of this protocol was validated by extensive simulations. The final solutions were clustered into ensembles A (40%), B (48%) and C (12%). The minor solution C could easily be excluded because in one conformer the two helices could not be linked by the trinucleotide bulge without causing steric collisions.

Cross-validation of the dynamical ensembles. Order tensors were predicted for each of the three TAR conformers in ensembles A and B by using Prediction of ALignmEnt from Structure (PALES)[34]. The order tensors for each helix were then averaged over the three conformers and resulting values compared with experimental counterparts[29]. Although solution A yields very good agreement between the predicted and measured helix order-tensor frames (Supplementary Fig. 5a) and RDCs (Supplementary Fig. 5a), the agreement is significantly less favourable for solution B (Supplementary Fig. 5b). The predicted S_{zz} deviates by 24° and 13° for HII and HI, respectively, and less favourable RDC agreement ($R = 0.89$) is observed (Supplementary Fig. 5b). Similarly, poor agreement was obtained for a motional model involving inter-conversion among all six conformers (data not shown).

Measurement and analysis of ^{15}N spin relaxation data in HIV-2 EI-TAR. Imino ^{15}N longitudinal (R_1), transverse ($R_{2(\mathrm{CPMG})}$) relaxation rates and {^{1}H}-^{15}N nuclear Overhauser effects (NOEs) were measured as described previously[13]. The relaxation delays for R_1 and $R_{2(\mathrm{CPMG})}$ experiments were 0.06, 0.12 (×2), 0.24, 0.48, 0.64, 0.80 (×2) and 1.2 s, and 0.0062, 0.0124 (×2), 0.0248, 0.0372, 0.0496, 0.0620 (×2) and 0.0744 s, respectively (duplicate measurements are denoted by '×2') (Supplementary Fig. 4a). Data were analysed by using the extended model-free formalism[35] (Supplementary Table 3) as implemented in Modelfree (Version 4.16 for Linux) from Palmer and co-workers[36], as described previously[13]. The RDC-derived HIV-2 EI-TAR inter-helix orientation was used as input structure for the model-free analysis.

32. Bailor, M. H. *et al.* Characterizing the relative orientation and dynamics of RNA A-form helices using NMR residual dipolar couplings. *Nature Protoc.* **2,** 1536–1546 (2007).
33. Saenger, W. *Principles of Nucleic Acid Structure* (Springer-Verlag, New York, New York, 1984).
34. Zweckstetter, M. & Bax, A. Prediction of sterically induced alignment in a dilute liquid crystalline phase; aid to protein structure determination by NMR. *J. Am. Chem. Soc.* **122,** 3791–3792 (2000).
35. Clore, G. M. *et al.* Deviations from the simple two-parameter model-free approach to the interpretation of nitrogen-15 nuclear magnetic relaxation of proteins. *J. Am. Chem. Soc.* **112,** 4989–4991 (1990).
36. Mandel, A. M., Akke, M. & Palmer, A. G. Backbone dynamics of *Escherichia coli* ribonuclease Hi: correlations with structure and function in an active enzyme. *J. Mol. Biol.* **246,** 144–163 (1995).